Electronic Supplementary Material (ESI) for Journal of Analytical Atomic Spectrometry.
This journal is © The Royal Society of Chemistry 2016

Electronic Supporting information

Imaging the 3D trace metal and metalloid distribution in mature wheat and rye grains via laser ablation-ICP-mass spectrometry and micro-X-ray fluorescence spectrometry

Stijn J.M. Van Malderen[1], Brecht Laforce[1], Thibaut Van Acker[1], Laszlo Vincze[1] and Frank Vanhaecke[1*]

[1]*Department of Analytical Chemistry, Ghent University, Campus Sterre, Krijgslaan 281 - S12, B-9000 Ghent, Belgium*

[*]*Corresponding author. E-mail address: Frank.Vanhaecke@UGent.be, phone number: +32 9 264 48 48, fax number: +32 9 264 4960*

Table of contents

Multimedia files

The paragraphs below discuss the distribution of every macro- and micronutrient as acquired using LA-ICP-MS analysis.

Phosphorus. In both *S. cereale* and *T. aestivum*, P is particularly prevalent in the aleurone layer, which is not surprising given its function as compartment for P storage (for germination) under the form of proteins, phytic acid, and phospholipids.[1-3] P is distributed evenly across the scutellum and embryo, and present at lower levels in the starchy endosperm.

Sulfur. S is one of the main plant nutrients and is found throughout the seed protein sinks in its role as a constituent of the amino acids methionine and cysteine, and in the form of glucosinolates, glutathiones and phytochelatins. The primary pathway towards S assimilation is based on the production of cysteine.[4] S is located fairly uniformly across the seed, with the relative concentration slightly higher in the embryo and sub-aleurone layer, in accordance with previous studies.[5, 6]

Cupper. Cu mainly accumulated in the scutellum and nucellar projection and at lower concentrations in the embryo and seed coat, whilst Mn, As, Cd, Cr, Ni and Pb show overall higher levels in the starchy endosperm, and lower doses in the scutellum and embryo. Cu has an essential role as the reducing or oxidizing agent in photosynthesis, mitochondrial respiration, carbon and nitrogen metabolism and oxidative stress protection. The complexation of Cu to small chaperone proteins and thiolate complexes allow Cu to accumulate.[7] Some biochemical reactions can be catalyzed using enzymes with Cu or Fe metal cofactors, e.g., Cu/Zn-superoxide dismutase (Cu/Zn-SOD) and Fe-superoxide dismutase; the distribution of Cu, Zn and Fe is remarkably similar, yet it is unclear why Cu accumulates more in the scutellum relative to the embryo.[8]

Manganese. Manganese is a cofactor in dozens of enzymes, as well as an activator; Mn thus represents a crucial function in the proteome.[7] In both grains, Mn is predominantly present in the outer perimeter of the primary and lateral roots (coleoptile/coleorhiza), scutellum, VB and the seed coat, as noted previously in literature.[5] In barley grains, the embryo contains high levels of Mn, Zn and Cu, while Fe and Mg concentrations were highest in the aleurone-containing fractions.[9] In Figure S-3e and Figure S-4e, elevated levels of Mn in the crease pericarp surrounding the VB can be observed. Similar observations were made by Neal et al. (2013) in mature wheat grains and by Lombi et al. (2011) in barley grains.[3, 9] Manganese-activated enzymes play a role in the nitrogen metabolism, gibberellic acid biosynthesis, RNA polymerase activation, and fatty acid biosynthesis.[7]

Zinc. Zn, a fairly mobile nutrient, is predominantly present in the embryo, intermediary layer at the scutellum-endosperm interface, with lower levels in the inner pericarp, aleurone layer, scutellum and trace levels in the endosperm.[10] The general pattern of TM sinks is similar across both grains, though significant differences exist as to the relative concentrations in these sinks between the genotypes. Wang et al. (2011) identified a transport barrier between the rachis and grains of *T. aestivum* by evaluating the bulk concentration at different development stages.[11] The presence of Zn in the aleurone layer is expected; EXAFS has shown Zn (and Fe) to be complexed with phytates and coordinated tetrahedrally by four O atoms and approximately 1.5 P atoms.[3] Zn-phytate complexes are stored in globoid crystals, which are protein storage vacuoles located in the aleurone layer and scutellum.[12, 13] Furthermore, Zn is omnipresent in large numbers of Zn-finger containing proteins and transcription factors, oxidoreductases, β-carbonic anhydrase, and hydrolytic enzymes, such as metalloproteases.[14, 15] Persson et al. (2009) suggested that the speciation of Zn in seeds correlates with the presence of proteins with the S-containing amino acids methionine and cysteine, whilst Fe (and P) are mainly associated with phytic acid.[1] Pongrac et al. (2013) exposed *T. aestivum* to Zn-enriched soil during grain filling, and as a result, Ca, Fe and Zn bulk concentrations increased significantly, whilst Na, P, Mg, Mn, Cu, Cd, K and Mo bulk concentrations decreased, supporting the hypothesis that Zn is competing to some extent with other metals (e.g., Cd, Na) for phytic acid.[16]

Cross-elemental patterns for macro- and micronutrients. Given the accumulation of Mn, Cu and Zn in the VB and NP regions, transport towards the filial tissue may be limited because of (i) the low sink capacity of the endosperm or (ii) the lack of sufficient transmembrane transporters. Sites of nutrient transfer, such as the crease VB and nucellar projection, can be distinguished. The gradient of Cu and Zn is similar, with accumulation towards the endosperm; the presence of some proteins, such as the Cu/Zn-SOD would explain this colocalization. The colocalization can also point towards shared transport pathways – Cu and Zn share transporters of the P_{1B}-type ATPase family – and storage systems (phytic acid), though the relative scutellum/embryo level ratio is significantly higher for Cu.[15] In the intermediary layer at the scutellum-endosperm interface, Zn is present at a higher level in *T.*

aestivum compared to the level of Zn in this layer in *S. cereale*, which indicates that the transport and storage pathways of the genotypes are not identical in this zone. In *S. cereale*, accumulation of Mn, Cu, P in the aleurone layer is accompanied by low concentrations in the endosperm. In the bran layers, P, Cu, Zn and Ni were located in the aleurone cells, whilst Mn and Pb was predominantly present in the seed coat. These elements appear to have a non-generic complexation mechanism, as the accumulation in the seed coat is exceptional. Gene expression of the micronutrient transporters, chelation agents and storage structures, e.g., the globoid crystals, are higher in the aleurone layer and embryo, resulting in accumulation of Fe and P into these sinks. Large concentration differences between the seed coat and epidermis suggest the presence of transport barriers, e.g., the cuticullar layer, between endosperm and epidermis. [17]

Table S-1 Abbreviation list for Regions-of-interest (ROIs)

Abbreviation	Definition of the ROI
P+PE	Testa (seed coat), pigment strand and pericarp (inner and outer)
SC	Scutellum
COL	Coleoptile
EN	Starchy endosperm
EM	Embryo
LP	Leaf primordia
IL	Intermediary layer at the scutellum-endosperm interface
AL	Aleurone layer
RP	Lateral root primordia
COZ	Coleorhizae

Figure S-1 Pixel assignment to the ROIs for (a) *Secale cereale* L. and (b) *Triticum aestivum* L.

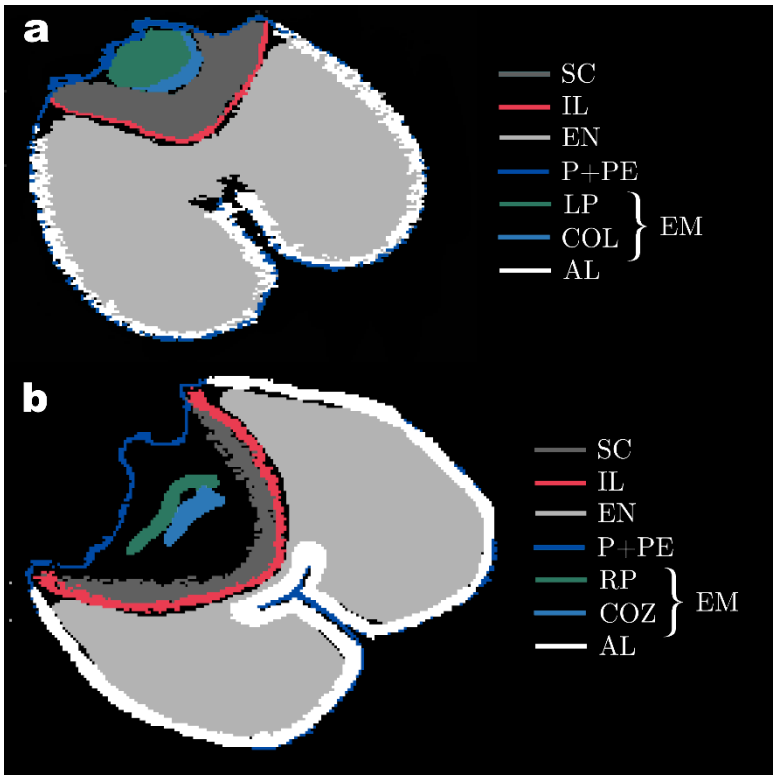

Figure S-2 RGB composites of metals and metalloids in *S. cereale* at the level of the root primordia (slice 19). The scale bar is 500 μm in length.

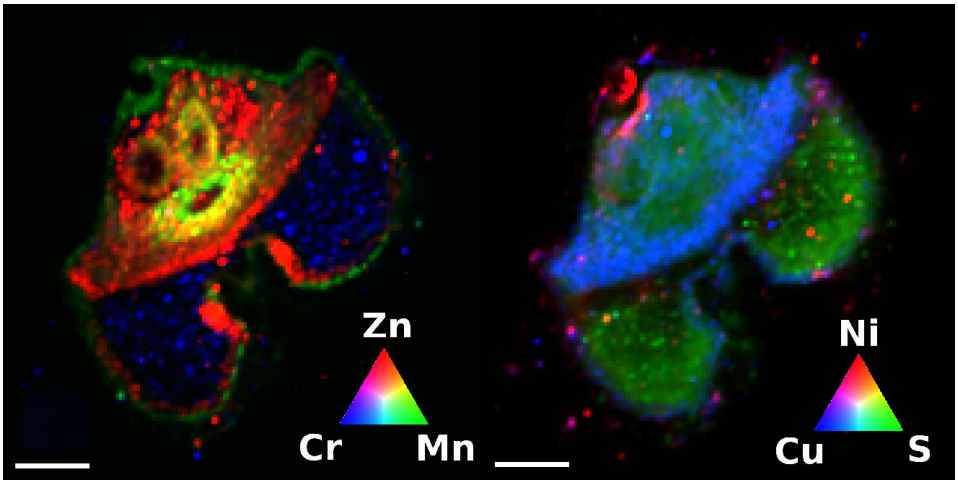

Figure S-3 Expanded version of Figure 2. LA-ICP-MS mappings of slice 19 of *Triticum aestivum* L. at the level of the root primordia. a) brightfield microscopy image of the grain. Annotations: embryo (EM), scutellum (SC), endosperm (EN), crease (CR), aleurone layer (AL), sub-aleurone layer (SAL), nucellar projection (NP), pericarp (PE), testa (P), coleorhizae (COZ), intermediary layer at the scutellum-endosperm interface (IL), root primordia (RP, primary and lateral roots), and vascular bundle (VB). (b-k) Individual elemental distributions as acquired by LA-ICP-MS. The images are scaled between 0 and the maximum intensity of the nuclide in counts per second. The scale bar in the lower left corner of each map is 500 μm in length.

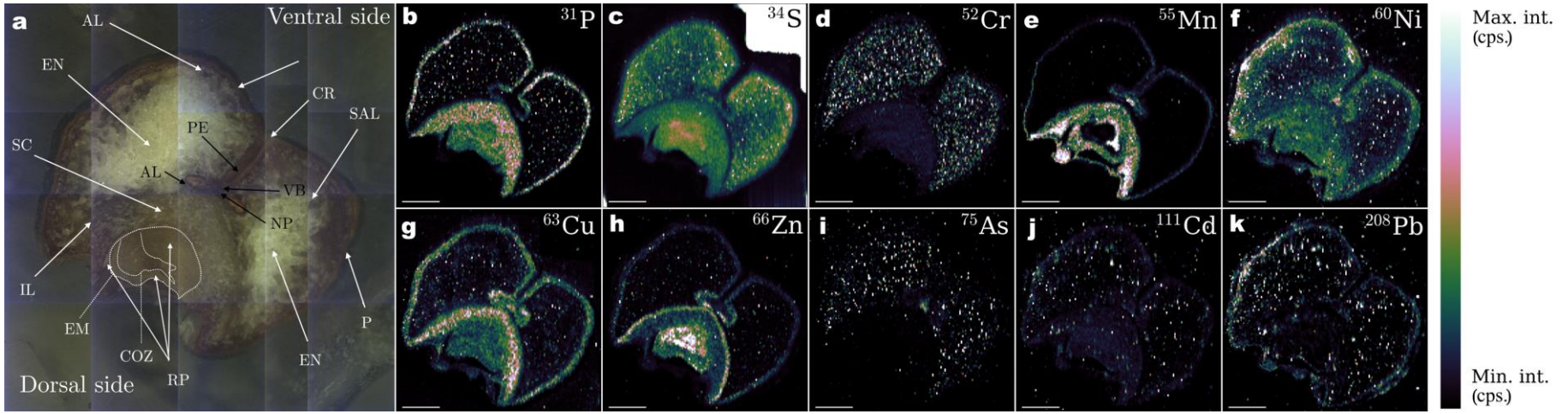

Figure S-4 Expanded version of Figure 3. LA-ICP-MS mapping of slice 16 of *Secale cereale* L. at the level of the leaf primordia (a) brightfield microscopy image of the grain. Annotations: embryo (EM), scutellum (SC), endosperm (EN), crease (CR), aleurone layer (AL), sub-aleurone layer (SAL), nucellar projection (NP), pericarp (PE), testa (P), leaf primordia (LP), coleoptile (COL), intermediary layer at the scutellum-endosperm interface (IL) and vascular bundle (VB). (b-k) Individual elemental distributions as acquired by LA-ICP-MS. The images are scaled between 0 and the maximum intensity of the nuclide

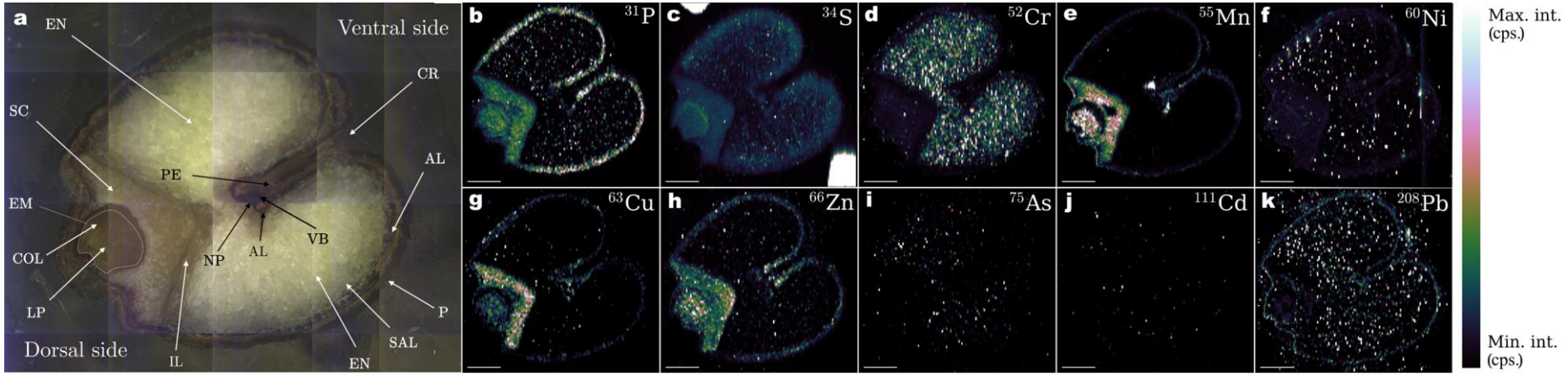

Figure S-5 Expanded version of Figure 4. a) Schematic illustration of the feature-based registration process, showing the transition from a set of 2D images towards a stack of aligned 2D images of the Cr distribution in *S. cereale*. b) 3D distribution of selected micronutrients in *T. aestivum* L. and a micro-CT image of the grain (voxel size $10 \times 10 \times 10\ \mu m^3$, 1000 projections, 1 s dwell time).

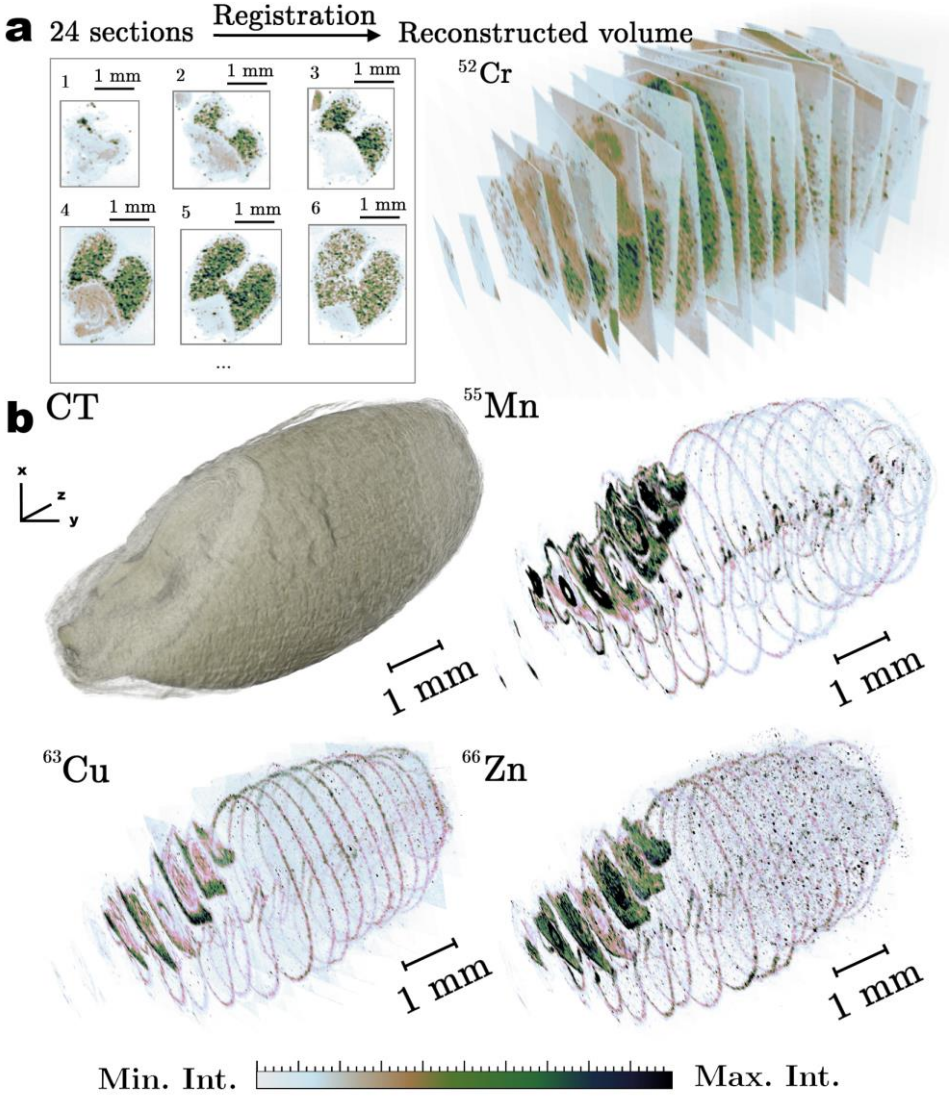

Table S-2 Average concentrations of heavy metals in $\mu g\, g^{-1}$ in *Secale Cereale* L. at slice 16, which contains the leaf primordia. The ROIs correspond with those indicated in Fig. S1. The precision is specified as 1 standard deviation (s). The list of abbreviations can be found in Table S-1.

Element	Cr	s	Mn	s	Ni	s	Cu	S	Zn	s	As	s	Cd	s	Pb	s	# Pixels in ROI
P+PE	2.1E-01	2.2E-03	4.7E+02	1.0E+01	1.4E+00	1.0E-01	2.3E+01	4.7E-01	7.5E+02	2.3E+01	2.7E-01	1.7E-02	5.4E-01	6.6E-02	6.3E-01	1.5E-02	1013
SC	2.3E-01	1.3E-03	1.2E+03	1.9E+01	1.1E+00	2.3E-02	5.5E+01	7.1E-01	1.9E+03	1.2E+02	3.2E-01	2.8E-02	1.1E+00	1.9E-01	3.1E-01	1.2E-02	1532
COL	5.2E-01	2.3E-01	2.1E+02	1.2E+01	1.3E+00	4.1E-02	2.0E+01	7.3E-01	1.7E+03	1.0E+02	3.3E-01	3.8E-02	5.6E-01	1.6E-01	2.1E-01	2.6E-02	157
EN	4.9E-01	1.7E-02	6.1E+01	3.0E+00	1.5E+00	8.0E-02	8.9E+00	1.2E-01	3.0E+02	7.1E+00	7.6E-01	2.9E-02	9.6E-01	3.6E-02	4.6E-01	1.3E-02	10250
EM	2.3E-01	1.5E-03	1.4E+03	4.6E+01	1.9E+00	3.9E-01	3.2E+01	5.3E-01	2.1E+03	6.1E+01	3.5E-01	5.2E-02	5.8E-01	5.6E-02	3.4E-01	1.2E-02	598
LP	2.3E-01	1.6E-03	1.4E+03	4.4E+01	1.3E+00	5.9E-02	3.3E+01	5.4E-01	2.1E+03	6.2E+01	3.7E-01	5.4E-02	6.7E-01	7.7E-02	3.4E-01	1.1E-02	587
IL	2.2E-01	3.7E-03	9.8E+01	6.2E+00	1.0E+00	1.5E-01	1.6E+01	5.9E-01	1.3E+03	7.0E+01	4.2E-01	6.0E-02	5.1E-01	9.4E-02	3.4E-01	5.1E-02	220
AL	2.4E-01	2.7E-03	2.3E+02	5.8E+00	1.5E+00	8.9E-02	2.4E+01	3.4E-01	1.2E+03	2.2E+01	3.5E-01	3.1E-02	5.5E-01	3.7E-02	4.5E-01	1.6E-02	1479

Table S-3 Average concentrations of heavy metals in *Triticum aestivum* L. in $\mu g\, g^{-1}$ at slice 19, which contains the root primordia. The ROIs correspond with those indicated in Fig. S1. The precision is specified as 1 standard deviation (s). The list of abbreviations can be found in Table S-1.

Element	Cr	s	Mn	s	Ni	s	Cu	S	Zn	s	As	s	Cd	s	Pb	s	# Pixels in ROI
P+PE	1.8E-01	2.7E-03	4.4E+02	1.3E+01	2.9E+00	7.5E-02	1.2E+01	2.1E-01	2.6E+02	8.3E+00	1.9E-01	3.2E-02	9.0E-01	6.0E-02	5.7E-01	2.0E-02	958
SC	2.3E-01	1.0E-03	1.1E+03	1.8E+01	2.6E+00	5.5E-02	2.6E+01	2.4E-01	6.6E+02	1.0E+01	9.3E-02	3.4E-03	1.2E+00	1.2E-01	3.2E-01	1.9E-02	1094
RP	2.2E-01	1.2E-03	1.1E+03	2.8E+01	2.7E+00	3.8E-02	1.1E+01	1.8E-01	1.1E+03	4.3E+01	5.8E-02	2.4E-03	1.1E+00	2.4E-02	2.1E-01	7.8E-03	253
COZ	2.3E-01	1.4E-03	2.4E+02	2.2E+01	2.9E+00	1.4E-01	1.2E+01	2.3E-01	2.5E+03	1.3E+02	4.8E-02	2.5E-03	1.2E+00	2.5E-02	2.2E-01	7.5E-03	198
IL	2.0E-01	1.3E-03	5.0E+02	2.3E+01	2.1E+00	3.3E-02	1.7E+01	3.0E-01	1.3E+03	2.4E+01	9.1E-02	9.2E-03	9.4E-01	1.8E-02	2.4E-01	6.5E-03	603
EM	2.2E-01	8.9E-04	7.3E+02	2.1E+01	2.6E+00	3.1E-02	1.1E+01	1.1E-01	1.4E+03	3.0E+01	6.7E-02	1.6E-03	1.1E+00	1.8E-02	2.4E-01	9.5E-03	1415
EN	3.2E-01	1.0E-02	2.3E+01	9.5E-01	2.1E+00	5.6E-02	5.1E+00	7.5E-02	1.4E+02	4.1E+00	3.1E-01	1.6E-02	8.1E-01	4.0E-02	3.4E-01	1.0E-02	8989
AL	2.0E-01	1.5E-03	2.5E+02	5.7E+00	3.3E+00	5.0E-02	1.5E+01	1.5E-01	4.5E+02	2.1E+01	1.8E-01	1.5E-02	1.2E+00	5.7E-02	5.8E-01	1.9E-02	2310

Figure S-6 Overview photograph of the spiked pellets.

Figure S-7 Photograph of ablation damage on the pellets. The scan line traverse the entire pellet.

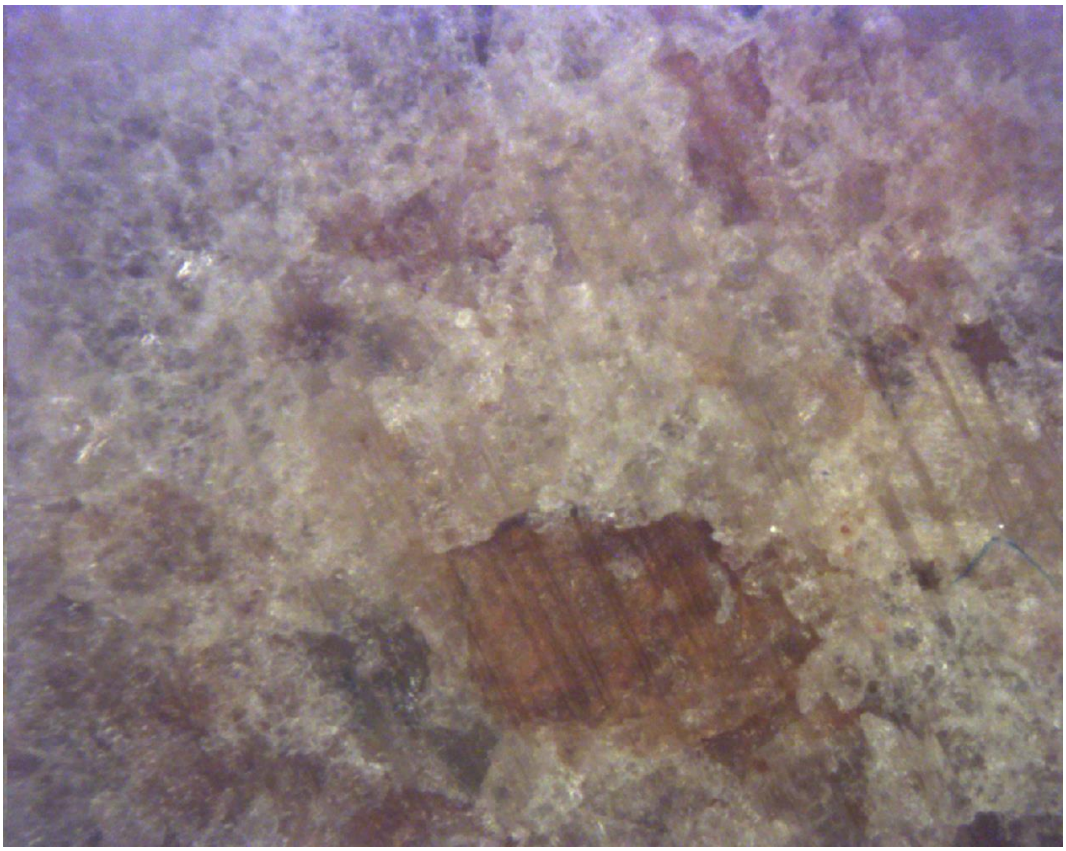

References

1. D. P. Persson, T. H. Hansen, K. H. Laursen, J. K. Schjoerring and S. Husted, *Metallomics*, 2009, **1**, 418-426.
2. L. Ozturk, M. A. Yazici, C. Yucel, A. Torun, C. Cekic, A. Bagci, H. Ozkan, H.-J. Braun, Z. Sayers and I. Cakmak, *Physiologia Plantarum*, 2006, **128**, 144-152.
3. A. L. Neal, K. Geraki, S. Borg, P. Quinn, J. F. Mosselmans, H. Brinch-Pedersen and P. R. Shewry, *Journal of Biological Inorganic Chemistry*, 2013, **18**, 557-570.
4. G. E. Ravilious and J. M. Jez, *Natural Product Reports*, 2012, **29**, 1138-1152.
5. A. P. Mazzolini, C. K. Pallaghy and G. J. F. Legge, *New Phytologist*, 1985, **100**, 483-509.
6. B. Wu, F. Andersch, W. Weschke, H. Weber and J. S. Becker, *Metallomics*, 2013, **5**, 1276-1284.
7. R. Hansch and R. R. Mendel, *Current Opinion in Plant Biology*, 2009, **12**, 259-266.
8. M. Pilon, S. E. Abdel-Ghany, C. M. Cohu, K. A. Gogolin and H. Ye, *Current Opinion in Plant Biology*, 2006, **9**, 256-263.
9. E. Lombi, E. Smith, T. H. Hansen, D. Paterson, M. D. de Jonge, D. L. Howard, D. P. Persson, S. Husted, C. Ryan and J. K. Schjoerring, *Journal of Experimental Botany*, 2011, **62**, 273-282.
10. T. J. Stomph, E. Y. Choi and J. C. Stangoulis, *Annals of Botany*, 2011, **107**, 927-937.
11. Y. X. Wang, A. Specht and W. J. Horst, *New Phytologist*, 2011, **189**, 428-437.
12. L. Bohn, A. S. Meyer and S. K. Rasmussen, *Journal of Zhejiang University Science B*, 2008, **9**, 165-191.
13. M. G. Palmgren, S. Clemens, L. E. Williams, U. Kramer, S. Borg, J. K. Schjorring and D. Sanders, *Trends in Plant Science*, 2008, **13**, 464-473.
14. U. Krämer and S. Clemens, in *Molecular Biology of Metal Homeostasis and Detoxification: From Microbes to Man*, eds. M. J. Tamas and E. Martinoia, Springer Berlin Heidelberg, Berlin, Heidelberg, 2006, **14**, 215-271.
15. I. Yruela, *Metallomics*, 2013, **5**, 1090-1109.
16. P. Pongrac, I. Kreft, K. Vogel-Mikus, M. Regvar, M. Germ, P. Vavpetic, N. Grlj, L. Jeromel, D. Eichert, B. Budic and P. Pelicon, *Journal of the Royal Society Interface*, 2013, **10**, 296-304.
17. J. W. Patrick and C. E. Offler, *Journal of Experimental Botany*, 2001, **52**, 551-564.